Assembly history and structure of galactic cold dark matter haloes

Wang, J.; Navarro, J. F.; Frenk, C. S.; White, S. D. M.; Springel, V.; Jenkins, A.; Helmi, A.; Ludlow, A.; Vogelsberger, M.

Published in:
Monthly Notices of the Royal Astronomical Society

DOI:
10.1111/j.1365-2966.2011.18220.x

Publication date:
2011

Monthly Notices
of the
ROYAL ASTRONOMICAL SOCIETY

Mon. Not. R. Astron. Soc. **413,** 1373–1382 (2011) doi:10.1111/j.1365-2966.2011.18220.x

Assembly history and structure of galactic cold dark matter haloes

J. Wang,[1]★† J. F. Navarro,[2] C. S. Frenk,[1] S. D. M. White,[3] V. Springel,[3,4,5] A. Jenkins,[1] A. Helmi,[6] A. Ludlow[7] and M. Vogelsberger[8]

[1]*Institute for Computational Cosmology, Department of Physics, University of Durham, South Road, Durham DH1 3LE*
[2]*Department of Physics and Astronomy, University of Victoria, Victoria, BC V8P 5C2, Canada*
[3]*Max-Planck-Institut für Astrophysik, Karl-Schwarzschild-Straße 1, 85740 Garching bei München, Germany*
[4]*Heidelberg Institute for Theoretical Studies, Schloss-Wolfsbrunnenweg 35, 69118 Heidelberg, Germany*
[5]*Zentrum für Astronomie der Universität Heidelberg, ARI, Mönchhofstr. 12-14, 69120 Heidelberg, Germany*
[6]*Kapteyn Astronomical Institute, University of Groningen, PO Box 800, 9700 AV Groningen, the Netherlands*
[7]*Argelander-Institut für Astronomie, Auf dem Hügel 71, D-53121 Bonn, Germany*
[8]*Harvard–Smithsonian Center for Astrophysics, 60 Garden Street, Cambridge, MA 02138, USA*

Accepted 2010 December 16. Received 2010 December 12; in original form 2010 August 30

ABSTRACT

We use the Aquarius simulation series to study the imprint of assembly history on the structure of Galaxy-mass cold dark matter haloes. Our results confirm earlier work regarding the influence of mergers on the mass density profile and the inside-out growth of haloes. The inner regions that contain the visible galaxies are stable since early times and are significantly affected only by major mergers. Particles accreted diffusely or in minor mergers are found predominantly in the outskirts of haloes. Our analysis reveals trends that run counter to current perceptions of hierarchical halo assembly. For example, major mergers (i.e. those with progenitor mass ratios greater than 1:10) contribute little to the total mass growth of a halo, on average less than 20 per cent for our six Aquarius haloes. The bulk is contributed roughly equally by minor mergers and by 'diffuse' material which is not resolved into individual objects. This is consistent with modelling based on excursion-set theory which suggests that about half of this diffuse material should not be part of a halo of *any* scale. The simulations themselves suggest that a significant fraction is not truly diffuse, since it was ejected from earlier haloes by mergers prior to their joining the main system. The Aquarius simulations resolve haloes to much lower mass scales than are expected to retain gas or form stars. Thus, the fraction of diffuse dark matter accreted by haloes represents a lower limit to the fraction of diffuse baryons accreted by galaxies. Our results thus confirm that most of the baryons from which visible galaxies form are accreted diffusely, rather than through mergers, and they suggest that only relatively rare major mergers will affect galaxy structure at later times.

Key words: methods: numerical – Galaxy: formation – dark matter.

1 INTRODUCTION

Hierarchical growth is a signature prediction of the Λ cold dark matter (ΛCDM) cosmogony, our current standard picture of cosmic structure formation. ΛCDM postulates a flat universe with a cosmological constant, cold dark matter and Gaussian initial conditions generated at very early times. The basic units of non-linear structure are dark matter haloes that grow by accretion and merging as gas cools and condenses into galaxies in their cores. The statistics of this process are amenable to analytic modelling, which can in turn be validated and extended through cosmological N-body techniques (see e.g. Press & Schechter 1974; Bond et al. 1991; Kauffmann & White 1993; Lacey & Cole 1993; Cole & Lacey 1996; Efstathiou et al. 1988; Jenkins et al. 2001).

The mass function of collapsed structure and its evolution with time, the clustering of haloes of different masses, the origin and character of scaling laws relating halo properties are all results that can be understood within the context of the excursion-set modelling making reference only to the initial power spectrum of density fluctuations and to the universal expansion history (see e.g. Lacey & Cole 1993; Mo & White 1996; Navarro, Frenk & White 1996).

The ΛCDM power spectrum, $P(k)$, can be computed in detail using linear theory. Under the simplifying assumption that the

★E-mail: wangjie@mpa-garching.mpg.de
†Newton International Fellow.

'temperature' of the dark matter is zero (or, equivalently, that the dark matter particle, if a thermal relic, has 'infinite' mass), $P(k)$ approaches k^{-3} on the smallest scales with a mass variance that diverges logarithmically there. Excursion-set theory then predicts that, at times of interest, effectively all of the mass of the Universe is in clumps of some mass. The assembly of a halo thus consists, in this simplified case, merely of the merging of the myriads of smaller mass subhaloes that collapsed at earlier times.

Under these conditions, merging is the basic engine of halo growth. The rapid mixing driven by the violently fluctuating potential of a merger has awesome transformative powers. Mergers can erase, at least partially, memory of the initial conditions and leave remnants whose broad structure is roughly independent of the cosmological conditions of formation (White 1978; van Albada 1982). Not all mergers, however, are created equal, and it has long been appreciated that the effects of major mergers differ qualitatively from those of minor events. In particular, major and minor mergers affect differently the internal structure of the remnant. Major mergers lead to 'rapid growth' in the mass of an object, which has been linked with radical changes in the halo structural parameters. Minor mergers, on the other hand, are associated with 'slow growth' evolutionary phases that leave the inner structure of the main halo relatively intact and affect mainly the periphery of the remnant (Salvador-Sole, Solanes & Manrique 1998; Wechsler et al. 2002; Zhao et al. 2003; Tasitsiomi et al. 2004; Diemand, Kuhlen & Madau 2007).

The idea of merging as the exclusive mechanism of halo growth has received some backing in the literature, most recently from Madau, Diemand & Kuhlen (2008), who report that most of the mass in their Via Lactea simulation of a galaxy-sized halo 'is acquired in resolved discrete clumps, with no evidence for significant smooth infall'. On the other hand, a number of recent papers have also argued that the fraction of mass accreted 'diffusely' might be substantial (see e.g. Angulo & White 2010; Fakhouri & Ma 2010; Genel et al. 2010, and references therein).

Angulo & White (2010), in particular, note that when a realistic CDM particle candidate is chosen, its small but non-negligible thermal velocity introduces a cut-off (and finite variance) in the power spectrum on small scales that can have a profound impact on the way the evolving hierarchy of collapsed structures develops. Working through the numbers appropriate for a neutralino-dominated Universe, these authors argue that, as late as $z \sim 20$, most of the mass of the Universe is not yet part of *any* halo. These authors also argue that a typical galaxy-sized halo accretes at least 10 per cent of its mass in diffuse form.

If these numbers are correct, the actual fraction of smoothly accreted material in a typical N-body halo must be much higher, since simulations can only resolve a limited range of non-linear scales and a fair fraction of the mass is expected to be locked up in unresolved small mass clumps. Angulo & White (2010) argue that, even in the best simulations currently available, up to 30–40 per cent of the mass of a galactic halo could have been accreted in diffuse form, in clear disagreement with the results of Madau et al. (2008). It is clearly important to resolve this disagreement, especially given the importance of diffuse mass accretion for galaxy formation emphasized in recent papers (see e.g. Kereš et al. 2005; Dekel et al. 2009, and references therein).

We address these issues here using the N-body simulations of the Aquarius Project (Springel et al. 2008a). This simulation series follows the formation of six different ΛCDM haloes at various resolutions and includes the best resolved galactic dark matter halo simulated so far, an object with more than one billion particles within the virial radius. We begin with a brief description of the Aquarius Project in Section 2, and move on in Section 3 to a systematic study of the radial structure of haloes in terms of the mass of their progenitor haloes and the time of their accretion/merging. Section 4 considers the mode of accretion into the haloes in detail and addresses the fraction of mass accreted in diffuse form. We end with a brief summary of our main conclusions in Section 5.

2 NUMERICAL SIMULATIONS

The Aquarius Project (Springel et al. 2008a) consists of a suite of large N-body simulations of six dark matter haloes of mass consistent with that expected for the halo of the Milky Way. Our simulations assume the ΛCDM cosmology, with parameters consistent with the *Wilkinson Microwave Anisotropy Probe* 1-yr data (Spergel et al. 2003): matter density parameter, $\Omega_{\rm M} = 0.25$; cosmological constant term, $\Omega_\Lambda = 0.75$; power spectrum normalization, $\sigma_8 = 0.9$; spectral slope, $n_{\rm s} = 1$; and Hubble parameter, $h = 0.73$.

The haloes were identified in a 900^3-particle N-body simulation of a cubic volume of $100\,h^{-1}$ Mpc on a side, a lower resolution version of the Millennium II Simulation (Boylan-Kolchin et al. 2009). This volume was resimulated using exactly the same power spectrum and phases of the original simulation, but with additional high-frequency waves added to regions surrounding the initial Lagrangian volume of each halo. The high-resolution region was populated with low-mass particles and the rest of the volume with particles of higher mass. These 'zoomed-in' simulations of selected regions or individual objects have become common practice to make galaxies; for details, we refer the reader to Power et al. (2003).

The six Aquarius haloes are labelled 'Aq-A' through 'Aq-F'. Each was resimulated at different resolutions in order to assess numerical convergence. A suffix, 1–5, identifies the resolution level, with level 1 denoting the highest resolution. Between levels 1 and 5, the particle mass ranges from $m_{\rm p} \sim 2 \times 10^3$ to $\sim 3 \times 10^6\,{\rm M}_\odot$. Level 1 was performed only for Aq-A and contains roughly 1.1 billion particles within the virial radius. All six haloes were simulated at level-2 resolution. Each of these has more than 100 million particles within the virial radius.

In this study, we analyse primarily the level-2 simulations but we also use lower resolution versions of Aq-A to test for numerical convergence. For the level-2 simulations, the particle mass is $m_{\rm p} \simeq 1 \times 10^4\,h^{-1}\,{\rm M}_\odot$ and the softening length is $\epsilon = 48\,h^{-1}$ pc. At $z = 0$, the six haloes have a similar 'virial' mass, $M_{200} \sim 1$–$2 \times 10^{12}\,h^{-1}\,{\rm M}_\odot$, where M_{200} is the mass contained within r_{200}, the radius of a sphere of mean density 200 times the critical density for closure.[1] The circular velocity curve of the haloes peaks at roughly $V_{\rm max} = 220 \pm 40\,{\rm km\,s^{-1}}$. For further details of the Aquarius Project, we refer the reader to Springel et al. (2008b) and Navarro et al. (2010).

At every snapshot in the simulation we find non-linear structures using the friends-of-friends (FOF) algorithm of Davis et al. (1985), with a linking length of 0.2 times the mean interparticle separation and 32 particles as the minimum number of particles per group. We then construct a merger tree for the final Aquarius haloes linking

[1] This choice defines implicitly the virial radius of the halo, r_{200}, and its virial velocity, V_{200}.

FOF progenitors at each time. We also identify bound substructures within each FOF halo (subhaloes) using the SUBFIND algorithm of Springel et al. (2005). Merger trees for subhaloes are constructed as described in Springel et al. (2008b).

For simplicity, unless otherwise explicitly noted, we shall identify a halo with the FOF structure that contains it. Note that the mass of FOF haloes does not necessarily coincide with the virial mass alluded to above (FOF structures are larger; they typically enclose a halo and a small part of its surroundings); we shall comment on these differences when appropriate in the analysis that follows.

Fig. 1 shows the growth of the FOF mass of the main progenitor of each halo, normalized to its value at the present time, $z = 0$. Merger events with mass ratio greater than $f_m = M_2/M_1 = 0.05$ are noted by vertical lines in the colour corresponding to the appropriate halo (scale on the right).

If we define the formation time of a halo as the time when the main progenitor first reaches half the final mass, then the formation time of the haloes is $z \sim 1.2$–2.2, except for halo Aq-F-2 which is clearly different from the rest. Its formation redshift is $z = 0.6$, when its mass almost doubles as a result of an almost equal-mass merger (the actual mass ratio of the two progenitors is $f_m = 0.75$). The other five haloes have similar mass growth histories but different merger histories. For example, haloes B, D and E experienced major mergers at high redshift ($z \sim 2$–7), while haloes A and C grew in a relatively quiescent fashion and did not experience any major mergers after $z = 6$. Although the Aquarius haloes have similar final masses, they have varied formation histories, which Boylan-Kolchin et al. (2010) has shown sample the range of behaviours seen in the Millennium II Simulation for haloes of this mass. The Aquarius haloes therefore provide a suitable sample to study the diversity in assembly histories of haloes similar to that surrounding the Milky Way.

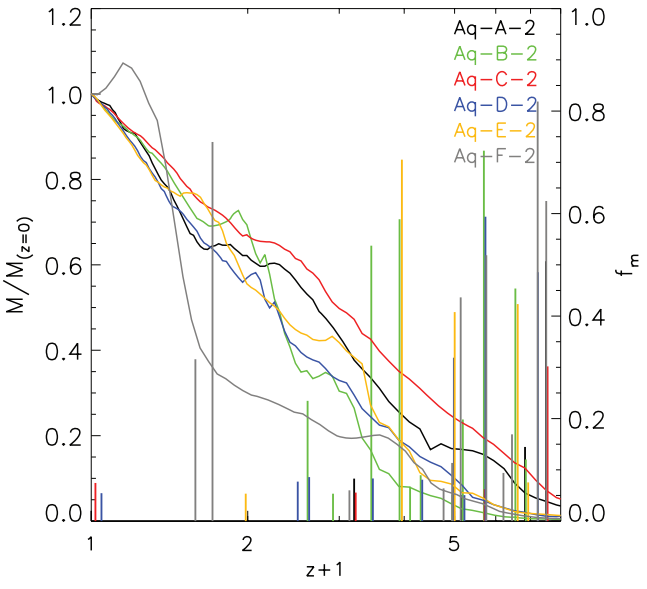

Figure 1. The evolution of the mass of the main FOF progenitor of the six level-2 Aquarius haloes. The curves show the mass in units of the mass at $z = 0$ (labels on the left y-axis). Vertical segments indicate the mass ratio of the largest merger event occurring at each snapshot (labels on the right y-axis). Only merger events with mass ratio exceeding 0.05 are shown. Colours identify individual haloes, as labelled in the figure. Note that only halo Aq-F-2 has undergone a major ($f_m > 0.1$) merger after $z = 1$.

3 MASS AND ACCRETION HISTORY

3.1 Mass growth and definition of accretion

Starting at $z = 0$ we identify the main trunk of the merger tree of each of our haloes by stepping back in time, defining the main progenitor at time $n - 1$ to be the largest FOF halo which is a progenitor of the main progenitor at time n. For each particle in the final object at $z = 0$, we register the redshift when it was accreted into the main progenitor (i.e. when it first ceased to be a single particle or a member of *another* FOF group), z_{acc}, and the mass of the FOF group, M_{prog}, to which it belonged at the snapshot immediately preceding the time of accretion. For 'diffuse' or 'smooth' accretion, terms we use interchangeably throughout, M_{prog} equals the mass of a single particle.

This seemingly straightforward definition of accretion is complicated by the fact that some particles can leave the main progenitor and be reaccreted again later on. This process can actually recur multiple times, and is usually associated with accretion events, where a small but non-negligible fraction of the mass is propelled into highly energetic orbits (Balogh, Navarro & Morris 2000; Gill, Knebe & Gibson 2005; Diemand et al. 2007; Ludlow et al. 2009).

There is therefore some ambiguity in the meaning of accretion time whose effects we illustrate in Fig. 2. Here we compare the growth of halo Aq-A using several plausible definitions of

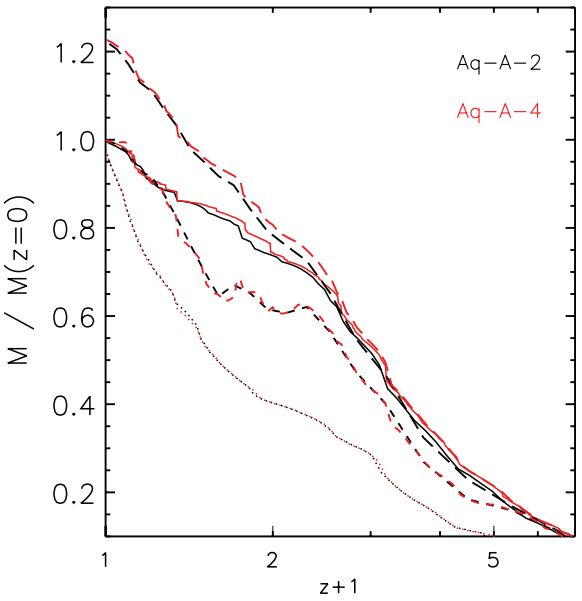

Figure 2. Mass accretion history of halo Aq-A. Curves in black correspond to the level-2 resolution halo and those in red to the level-4 run. All masses are normalized to the FOF mass of the halo at $z = 0$. Four definitions of halo mass build-up are compared. The long-dashed (top) curves indicate the mass of all particles 'associated' with the halo; i.e. those that were part of the main progenitor at *any time* before redshift z. The dotted (bottom) curves are the mass of particles that belong to the most massive progenitor *at all times* after z (i.e. after the time of last accretion). The thin solid curves (second set from top) indicate the cumulative mass of particles as a function of the redshift of *first* accretion into the main progenitor (regardless of whether they leave and re-enter the main progenitor subsequently). The short-dashed curves indicate the conventional FOF mass of the main progenitor at each time. This comparison illustrates the fact that a significant fraction of the mass of the main progenitor is pushed out of the halo boundary during its evolution; much of it is reaccreted later, but more than 20 per cent is still outside the main halo at $z = 0$.

accretion and two different levels of resolution to check for possible numerical artefacts. The dashed curves (second from the bottom) track, as in Fig. 1, the conventional FOF mass of the main progenitor, normalized to its value at $z = 0$. The long-dashed curves (top) show, on the other hand, the cumulative mass of all particles that, at any time before z, have been part of the main progenitor. These 'associated' particles exceed the FOF halo at $z = 0$ by more than 20 per cent, highlighting the importance of the energy redistribution process described in the previous paragraph.

The solid thin curves, on the other hand, track the $z = 0$ FOF particles, but use the time of *first* accretion to define z. The difference between this and the conventional FOF mass is a direct indicator of the accretion-escape-reaccretion process alluded to above. Finally, the dotted (bottom) curves use the time of *last* accretion of particles in the $z = 0$ FOF group. Fig. 2 shows clearly that a halo is a dynamic object and not a static 'bucket' of mass that gets progressively filled by accretion. For simplicity, we shall in what follows adopt the time of first entry as our default definition of accretion but we caution that other definitions of accretion may on occasion be more useful, depending on the aim of the analysis. The good agreement between the results for Aq-A-4 and Aq-A-2 shows that these conclusions are insensitive to the numerical resolution of the simulations.

3.2 Progenitor mass distribution as a function of radius

We now investigate the fate of particles accreted in progenitor haloes of different masses. More specifically, we investigate the distribution of halo mass in spherical shells (centred at the location of the minimum in the gravitational potential) and apportion the contribution according to the mass, $M_{\rm prog}$, of the subhaloes that brought each particle into the main progenitor.

This is shown in Fig. 3, which gives, in each panel, the fraction of particles in concentric radial shells of each $z = 0$ Aquarius halo, split into six mass bins, according to the mass of the progenitor halo at the time of accretion. Each bin is identified by a different colour according to the key to the right of each panel. This key, in addition, gives the total fraction (summed over all radial shells) of mass brought in by progenitors of different masses. Material that was already in place at $z = 6$ (when few resolved progenitor haloes exist) is indicated in grey; in this section and the next, we do not consider the assembly history at earlier times. Particles that in the snapshot preceding accretion are unattached to any resolved halo (i.e. diffuse accretion) are indicated in red.

Fig. 3 shows that there is considerable halo-to-halo variation in the mass spectrum of the progenitors of the final halo. Consider, for example, the integrated halo mass. As the key to the right of each panel shows, the fraction of mass that was already in place at $z = 6$ ranges from ∼5 to ∼15 per cent. The fraction of mass accreted diffusely is substantial in all cases, ranging from ∼30 to ∼40 per cent. The diffuse fraction increases with radius, from a few per cent within $10\,h^{-1}$ kpc to more than 20 per cent within $100\,h^{-1}$ kpc. This agrees with the results found by Helmi, White & Springel (2002) from an N-body simulation of a cluster halo scaled to a galactic mass. The radial behaviour is diverse. For example, in haloes A and C the material in the innermost region, $r < 1$ kpc, was already in place before $z = 6$ and has undergone little change since. By contrast, in haloes B, E and F, most of the central mass was brought in after $z = 6$ through mergers involving host haloes with mass greater than $10^{10}\,h^{-1}\,{\rm M}_\odot$.

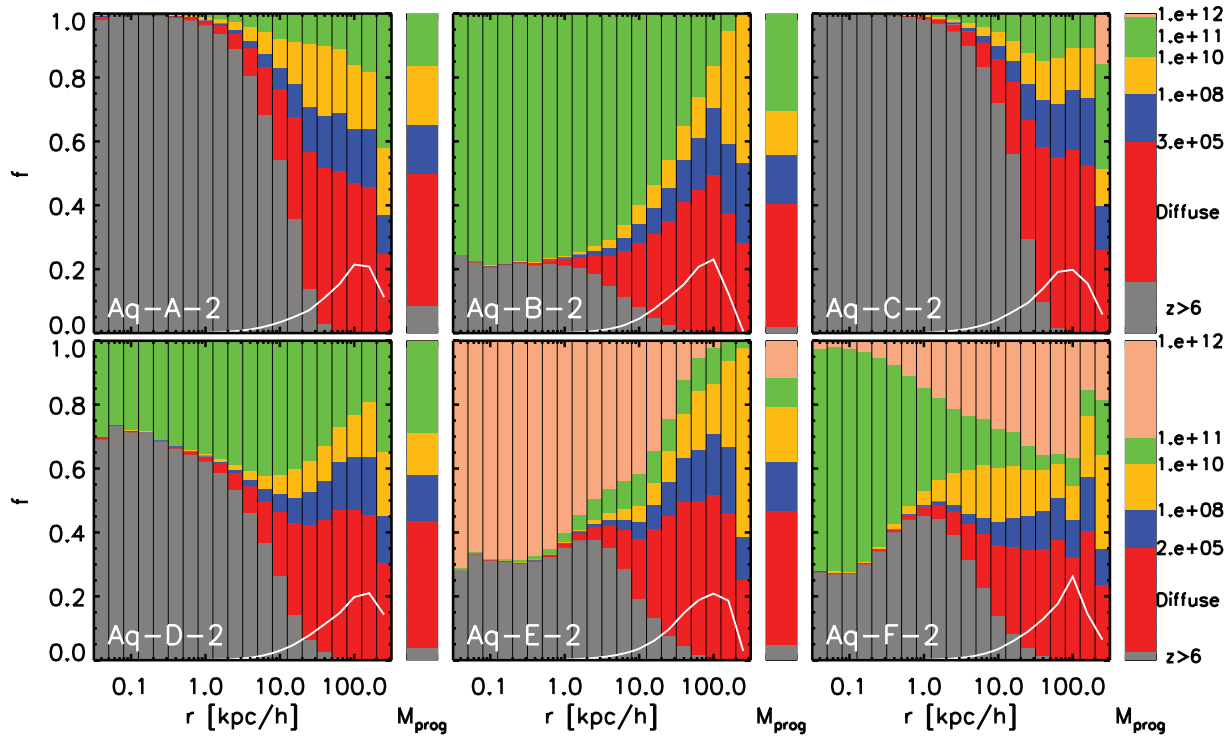

Figure 3. The radial distribution of particles in the FOF $z = 0$ halo colour-coded according to $M_{\rm prog}$, the mass of the progenitor to which each particle belonged at the time of (first) accretion into the main halo. The bars represent the fraction of the mass in each spherical shell brought in by haloes with mass in the range indicated by the key to the right of each panel. This key also gives the total fraction (summed over all radial shells) of mass brought in by different progenitors. Material accreted before $z = 6$ is indicated in grey. Diffuse material, that is, particles that were not part of any FOF halo at the time of accretion, is indicated in red. Masses are in units of $h^{-1}\,{\rm M}_\odot$. The white curve gives the fraction of the total FOF halo mass in each radial shell.

Halo D is intermediate between these two extremes. Large progenitors, of a mass of $>10^{10}\,h^{-1}\,\mathrm{M}_{\odot}$, bring in between 20 and 40 per cent of the final mass at all radii. In general, the larger the mass of the carrier halo, the greater the probability of the particles ending up in the central regions. Very little of the diffuse material makes it into the central regions, $r < 10\,h^{-1}$ kpc; indeed, most of it stays in the outer regions where it typically contributes most of the mass.

3.3 Accretion time distribution as a function of radius

We now turn our attention to the radial distribution of particles as a function of their accretion time. Analogously to Fig. 3, Fig. 4 shows the distribution of accretion redshifts, binned according to the distance to the centre of the halo. In each radial shell, the contribution from material accreted in different time intervals is shown by strips coloured according to the key shown to the right of each panel. The key also gives the fractions of the total halo mass (summed over all shells) accreted in each redshift interval.

The inside-out nature of halo assembly is clearly apparent in Fig. 4. On average, the peak contribution from each accretion redshift interval marches outwards with time. The inner regions are populated mostly by particles that were accreted early; the outer layers were added gradually later. The cores of haloes A and C were in place before $z = 6$ and evolved little thereafter. In haloes D, E and F, the core particles were accreted by $z = 3$, but for halo B, the core is accreted at $z = 1$ because two major mergers in the redshift interval $1 < z < 3$ bring in almost 50 per cent of the core mass (see Fig. 1). These mergers happen relatively early, while the total halo mass is small, and disrupt the original core which then reforms from the new material. By contrast, the late major merger undergone by halo F has a relatively minor effect on the core, probably because of the orbital parameters of the merger. The core in this case is actually made primarily out of material that was accreted in earlier, lesser mergers at $z \sim 4$.

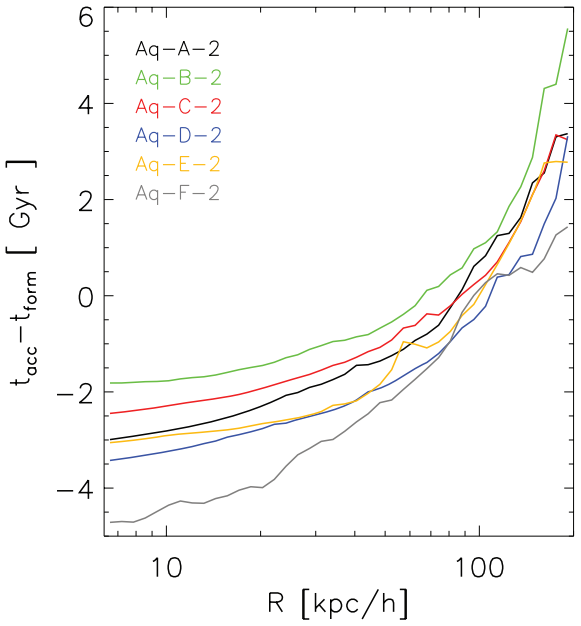

Figure 5. The mean accretion time of particles in different radial shells at $z = 0$. Accretion times are shown relative to the formation time of each halo, t_{form}, defined as the time when the halo first reached half its final mass. When defined this way, the mean accretion time profile is similar for all Aquarius haloes.

The radial dependence of accretion time is quantified further in Fig. 5, which shows the average accretion time as a function of

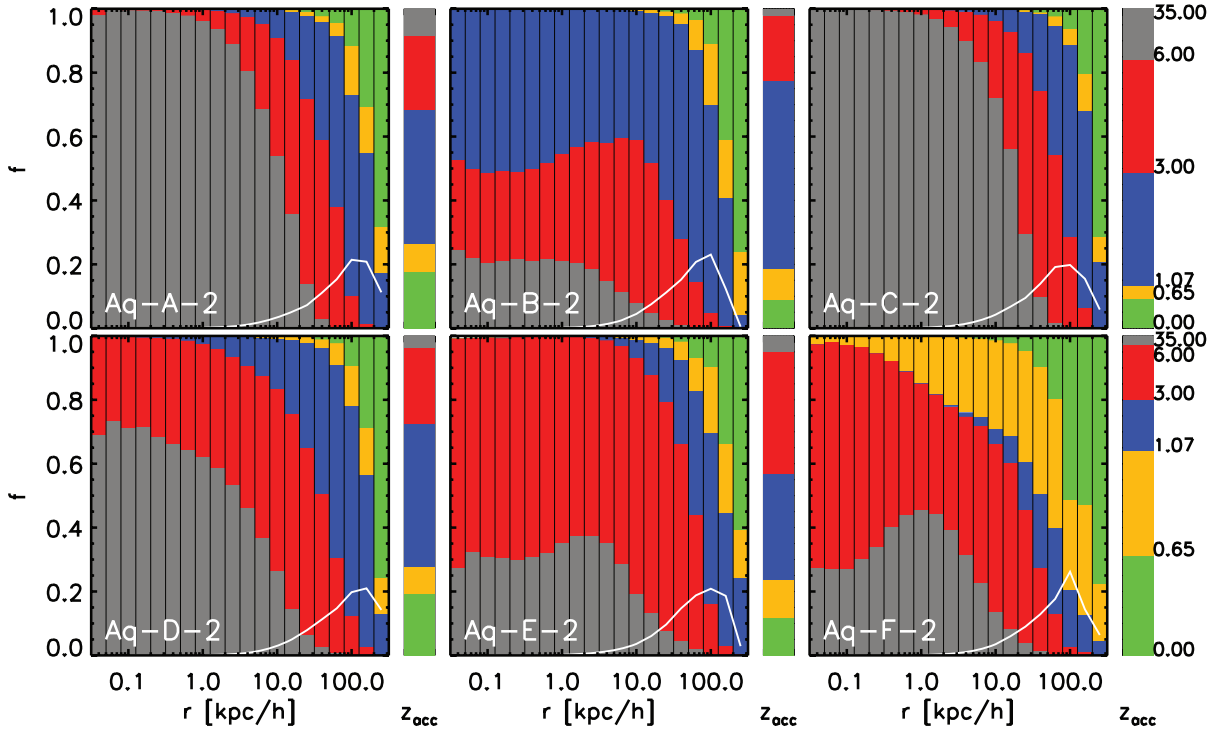

Figure 4. As Fig. 3, but for z_{acc}, the redshift of (first) accretion of particles into the main halo. Different colours indicate accretion redshift in the intervals indicated by the key to the right of each panel. This key also gives the total mass fraction (summed over all radial shells) accreted in each redshift interval. The white curve gives the fraction of the total FOF halo mass in each radial shell.

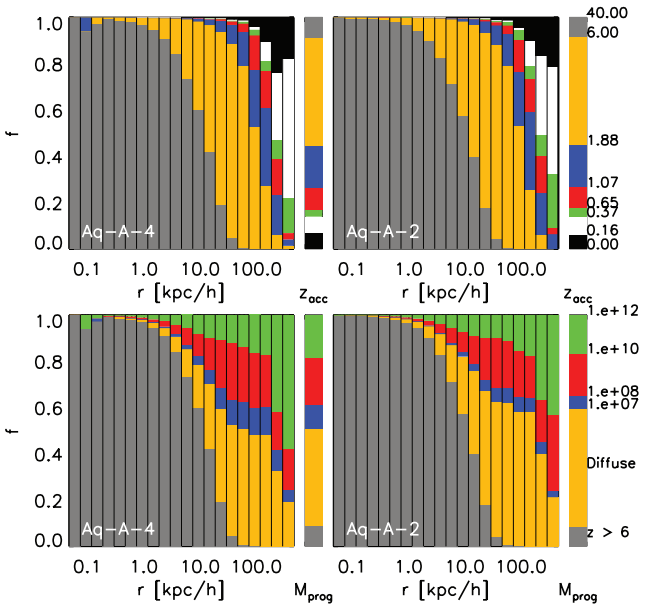

Figure 6. A convergence test of the radial gradients in progenitor mass and accretion redshift. The top two panels are analogous to Fig. 4 and the bottom panels to Fig. 3, but for the level-2 and level-4 Aq-A runs. These runs differ solely in numerical resolution; level-2 runs have 30× more particles and 5× smaller gravitational softening than their level-4 counterparts. The excellent agreement shows that the results presented in Figs 3 and 4 are insensitive to numerical resolution.

radius. Accretion time is plotted relative to the formation time of the halo, $t_{\rm form}$, defined as the time when the main progenitor first reaches half its final mass. With this normalization, the radial dependence of the accretion time is fairly similar for all Aquarius haloes. On average, the material in the inner $10\,h^{-1}$ kpc is assembled 2–4 Gyr before $t_{\rm form}$ whereas the material beyond $100\,h^{-1}$ kpc falls in 2–4 Gyr after $t_{\rm form}$. This onion-like growth is generic for CDM haloes of galactic scale; it was also seen in a scaled cluster N-body simulation by Helmi, White & Springel (2003).

3.4 Numerical convergence

Before discussing these results further, we should verify that the trends presented above are not unduly influenced by numerical resolution. The availability of simulations of the same halo at varying resolutions allows for direct testing of the reliability of our results. We do this by comparing the level-2 simulation of halo Aq-A, which is the one we have analysed so far, with its level-4 counterpart. The level-4 simulation has about 30× poorer mass resolution and 5× poorer spatial resolution (softening).

The test is carried out in Fig. 6, which shows the distributions of accretion time and the mass spectrum of progenitor haloes as a function of radius. These figures are analogous to Figs 3 and 4. The left-hand panels show the level-4 results and the right-hand panels show the level-2 results. It is clear that the convergence of these properties is excellent. There is no discernible difference in the distributions of $z_{\rm acc}$ and at most an ∼10 per cent difference in the distributions of $M_{\rm prog}$ in the lowest mass range, $M_{\rm prog} < 10^7\,h^{-1}\,{\rm M}_\odot$.

4 MODES OF ACCRETION

In this section we study how the growth of haloes is apportioned between major mergers, minor mergers and smooth accretion; how the material added in these modes is distributed in radius in the final haloes; and how much variation there is between haloes. We will adopt an FOF mass ratio of 10:1 as our standard division between major and minor mergers, although we will also give some results for the stricter 3:1 ratio adopted as a boundary by some authors. The fact that we limit our FOF group catalogues to systems with at least 32 particles means that the boundary between minor mergers and 'smooth' accretion occurs at a mass ratio of about $10^{6.5}$:1 at $z = 0$ dropping to about $10^{5.5}$:1 at $z = 4$ and to even smaller values at higher redshifts. In this section we consider increases in mass through each of these growth modes throughout the entire history of each halo, rather than halting at $z = 6$ as in previous sections.

4.1 Major mergers versus minor mergers

In Fig. 7 we illustrate how major mergers, minor mergers and diffuse accretion contribute to the $z = 0$ mass in a series of spherical shells, each spanning a factor of 2 in radius. The symbols joined by lines give results averaged across the six Aquarius haloes, while the error bars indicate the rms scatter among haloes. Within $\sim 10\,h^{-1}$ kpc, major mergers are the dominant source of the material, providing typically 40 per cent of the mass, while minor mergers and smooth accretion bring in about 30 per cent each, respectively; within $\sim 1.0\,h^{-1}$ kpc, major mergers contribute more than two-thirds of the mass. Note, however, that less than 10 per cent of halo mass lies within $\sim 10\,h^{-1}$ kpc and less than 1 per cent lies within $\sim 1.0\,h^{-1}$ kpc. Note also from Fig. 4 that the great majority of these major mergers occurred at $z > 3$ and many of them at $z > 6$. Only in haloes B and F are there substantial contributions to these regions from major mergers at redshifts below 3. The large error

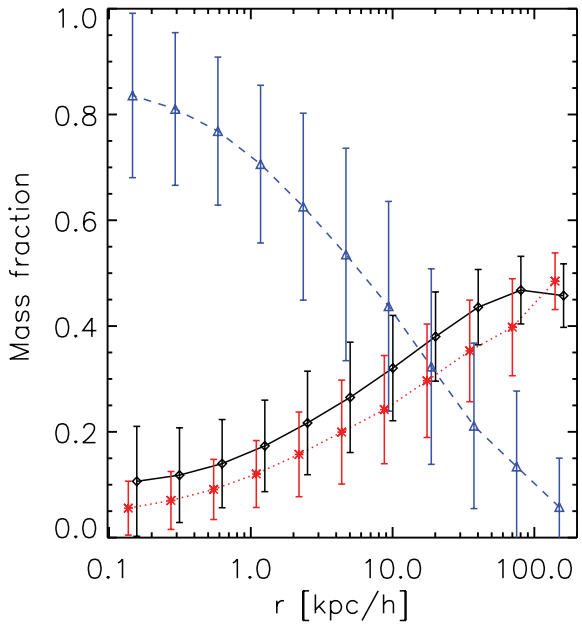

Figure 7. The fraction of particles in a series of spherical shells that were accreted smoothly (black circles – solid line), by minor mergers (starred symbols – dotted) and by major mergers (open triangles – dashed). The distinction between minor and major mergers is made at a mass ratio of 10:1. Fractions are averaged over all six level-2 Aquarius haloes and error bars show the rms scatter among haloes. Despite substantial scatter, the trends are clear. Major mergers contribute to the inner regions, and diffuse accretion and minor mergers mainly to the outer regions which contain the bulk of the mass.

bars on these points indicate that the scatter of the major merger contribution to the inner regions of haloes is large.

Beyond $10\,h^{-1}$ kpc, in the region which contains the bulk of the halo mass, both minor mergers and diffuse accretion contribute more to halo growth than major mergers. Indeed, averaged over all six haloes, major mergers contribute only 17 per cent of the total mass growth, with the values for individual haloes ranging from 3 per cent (Aq-A) to 36 per cent (Aq-F). For a stricter definition of a major merger, requiring a mass ratio of 3:1 or less, the mean major merger contribution drops to just 9 per cent, with individual values ranging from <0.1 per cent (Aq-A, Aq-C) to 25 per cent (Aq-F). Thus, major mergers are typically a small contribution to overall halo growth. The rest is split almost evenly between minor mergers and 'diffuse' accretion. It is interesting that the scatter in each of these contributions is very close to half of that in the major merger contribution. This shows that the minor merger and diffuse fractions fluctuate up and down together, with minor mergers contributing slightly less than half of the material not accounted for by major mergers at each radius and in each halo.

4.2 Diffuse accretion

Given the conflicting claims in the literature regarding the importance of diffuse accretion discussed in Section 1, it is important to explore possible biases and subtleties involved in reckoning the amount of diffuse mass accreted. The dynamic nature of halo build-up highlighted in Section 3.1 introduces ambiguities in the meaning of accretion, so we compare the following four alternative definitions of $f_{\rm smooth}$, the total fraction of mass in the FOF halo at $z = 0$ that has been added smoothly:

I. all particles that were not part of *any* 32+ particle FOF group *in the snapshot immediately before* the time of first accretion, $z_{\rm acc}$;
II. all particles that were never part of *any* 32+ particle *bound* structure (as identified by SUBFIND) before $z_{\rm acc}$;
III. same as II but for 20+ particles;
IV. same as I but for *all* snapshots before $z_{\rm acc}$.

Fig. 8 compares results for the six level-2 Aquarius haloes. Criterion I, probably the simplest, is seen to give the largest estimate of $f_{\rm smooth}$ in all cases. This criterion omits those particles that were part of FOF haloes in the past but that have left them and are unattached to any resolved structure just before accretion. These make a surprisingly large fraction (about *half*!) of the smooth fraction computed using criterion I, as shown by the bottom curve corresponding to criterion IV.

One shortcoming of criterion IV, however, is the possibility that FOF groups may artificially link in physically unrelated particles. This is especially true in small-N groups (for a recent discussion, see e.g. Bett et al. 2007). Criteria II and III account for this by requiring particles to be part of *bound* structures; varying the threshold from 20 to 32 particles has negligible effect on the results. This extra condition is seen to increase $f_{\rm smooth}$ by roughly 50 per cent relative to criterion IV. The contribution of diffuse accretion seems therefore to be genuinely high, between 20 and 40 per cent of the final halo mass overall.

We note that, strictly speaking, $f_{\rm smooth}$ depends on the total number of snapshots used in its estimation. The numbers quoted above are based on a total of 128 snapshots, but for one of the runs (Aq-A-4) data were stored for 1024 snapshots. The estimate of $f_{\rm smooth}$ according to criterion I changes little when considering 1024 or 128 snapshots: from 41 to just 36 per cent. The changes are even smaller for definition II or III.

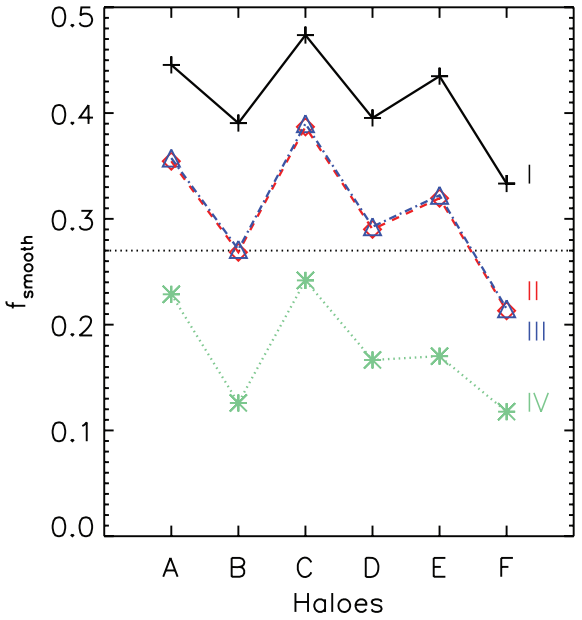

Figure 8. The fraction of mass accreted in diffuse form in each level-2 Aquarius halo. The x-axis lists the name of each halo. Each curve corresponds to one of the definitions of 'diffuse accretion' introduced in the text. Briefly, I are particles that are unattached to any FOF group identified in the snapshot immediately before first accretion, II refers to particles that do not belong to any *bound* structure with ≥32 members in *any* snapshot before first accretion, III is as II but for 20 members and IV denotes material that did not belong to *any* $N \geq 32$ FOF group at any time before first accretion. All curves use a total of 128 snapshots to estimate $f_{\rm smooth}$. The excursion-set prediction for a halo of the same mass and comparable numerical resolution is shown by the horizontal dotted line.

Finally, we consider the dependence of $f_{\rm smooth}$ on the mass resolution of the simulations. For this, we use four different realizations of halo Aq-A, from level 2 to level 5. The results are shown in Fig. 9 (criteria II and IV: open diamonds and asterisks, respectively). As expected, there is a systematic decrease in $f_{\rm smooth}$ with increasing resolution, measured in Fig. 9 by $M_{\rm cut}$, the mass of a group of 20 particles.

Given that $f_{\rm smooth}$ depends on resolution, we need to ask how secure is our estimate of this quantity from the simulations. We can answer this by analysing Monte Carlo merger trees built using the excursion-set formalism, constrained at $z = 0$ to make a halo of mass comparable to those in the Aquarius set. In particular, we use the algorithms of Parkinson, Cole & Helly (2008) and Cole et al. (2008), which were tuned to match the N-body merger trees of the Millennium Simulation (Springel et al. 2005). This approach has the advantage that a cut-off mass can be easily introduced in order to mimic the limited resolution of a simulation (see e.g. Angulo & White 2010).

The excursion-set results are shown by the dotted line in Fig. 8 and by the connected dots in Fig. 9. The Monte Carlo trees, when trimmed to match the resolution of the N-body simulations, give results in good agreement with the simulations. The theoretical calculation also confirms the large scatter in $f_{\rm smooth}$ seen in the simulations. (The 'error bars' on the Monte Carlo results denote the rms scatter among several hundred realizations.)

The trends shown in Fig. 9 imply that further improvements in resolution would result in only small reductions in the value of $f_{\rm smooth}$. Indeed, $f_{\rm smooth}$ seems to depend more strongly on the particular definition adopted for smooth accretion than on numerical

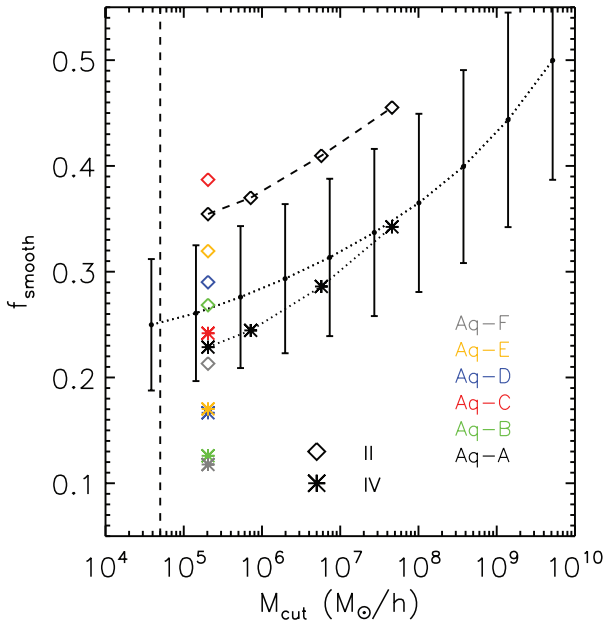

Figure 9. The dependence of the diffuse accretion fraction, $f_{\rm smooth}$, on the mass resolution of the simulations, $M_{\rm cut}$, defined as the mass of a group of 20 particles. Open diamonds and asterisks refer to diffuse accretion definitions II and IV, as described in the text and in the caption to Fig. 8. Connected symbols refer to resolution levels 2–5 for halo Aq-A. Colours indicate different haloes, as labelled in the panel. Dots with error bars indicate the mean and rms scatter in several hundred Monte Carlo assembly histories constructed from excursion-set theory. The vertical dashed line indicates the value of $M_{\rm cut}$ for Aq-A-1, the highest resolution simulation in the Aquarius series.

resolution, at least for the 100-million particle haloes we consider here. The vertical dashed line in Fig. 9 shows the value of $M_{\rm cut}$ corresponding to Aq-A-1, the best resolved, billion-particle halo in the Aquarius set. The Monte Carlo tree results suggest that its additional resolution would result in only a very small decrease in the smoothly accreted fraction.[2]

We conclude from this exercise that the substantial fraction of mass found to be accreted smoothly in our simulations is a robust result. We can therefore confidently rule out the claim by Madau et al. (2008) that at most 3 per cent of the mass of a galaxy-sized halo can be supplied by smooth accretion. It is not clear at this point what the cause of the disagreement is, but it is likely to be related to the way in which these authors compute diffuse accretion rather than to differences in the simulations themselves. For example, the mass they regard as having been accreted in 'identifiable subunits' is just the sum of the masses of all progenitor haloes that contain particles that make it into the final system. A substantial fraction of that summed mass includes particles that are *not* part of the halo at $z = 0$; this could have led Madau et al. (2008) to overestimate the mass contributed by discrete identifiable subunits and therefore to underestimate $f_{\rm smooth}$.

Our conclusions are in agreement with those of Angulo & White (2010) (see also Genel et al. 2010): mergers *and* smooth accretion are both defining features of the hierarchical build-up of a CDM halo.

[2] We have not attempted the analysis presented here for Aq-A-1 because of the formidable computational task involved in building full merger trees for this simulation.

The fraction of dark mass accreted diffusely can be thought of as a lower limit to the fraction of baryons accreted diffusely into visible galaxies. At redshifts below ∼6, the intergalactic medium is fully photoionized and gas is unable to collect in haloes with maximum circular velocity below about 15 km s^{-1}. This corresponds to masses below $\sim 10^8\,{\rm M}_\odot$ (see e.g. Okamoto, Gao & Theuns 2008), which is well above the resolution limit of our simulations. Therefore, the baryons associated with these low-mass haloes should be considered to be diffusely accreted along with the baryons associated with the 'diffuse' dark matter. Taking the limit at exactly $10^8\,h^{-1}\,{\rm M}_\odot$ for simplicity,[3] we find that, on average, our haloes accrete 56 per cent of their baryons diffusely, with the numbers for individual haloes ranging from 46 per cent (Aq-F) to 64 per cent (Aq-C). The bulk of baryonic accretion is thus predicted to be smooth rather than clumpy for objects of the Milky Way scale.

4.3 Evolution of the inner mass profile

As Fig. 7 indicates, major mergers contribute, on average, just under half of the particles in the inner $10\,h^{-1}$ kpc of Galactic haloes. This is the region occupied by the luminous component of the central galaxy, and it is thus interesting to analyse in detail how the mass profile in this region evolves with time. A thin stellar disc, for example, could react to clumpy addition of material by thickening and becoming dynamically hotter, potentially violating observations of the thin disc in the solar neighbourhood (see e.g. Benson et al. 2004).

We investigate the stability of the inner halo explicitly in Fig. 10, where we plot the mass enclosed within 1, 2, 8 and 32 (physical) kpc[4] from the centre of each halo as a function of time. Each curve is normalized to the enclosed mass at $z = 0$. Except for halo F, which undergoes a major merger at $z \sim 0.6$, all the haloes show exceptionally stable inner mass profiles over at least the past 5 Gyr ($z < 0.6$), the age of the Solar system. Five out of six Aquarius haloes could, in principle, host a disc as thin and cold as that of the Milky Way. Late-accreted mass typically settles in the outskirts of a halo, thus allowing the hierarchical growth of haloes to be reconciled with the ubiquitous presence of thin stellar discs.

5 SUMMARY AND CONCLUSIONS

We have analysed the build-up of six ΛCDM haloes simulated as part of the Aquarius Project to study the influence of assembly history on halo structure. We focus on the distributions of progenitor mass and accretion time for particles at different radii at the final time, and discuss various plausible definitions of accretion time, together with the difficulties involved in estimating the total mass fraction accreted smoothly. We compare simulations of the same halo carried out with different resolutions in order to assess the sensitivity of our results to numerical limitations.

Although there is considerable variation from halo to halo, our simulations exhibit a number of very clear trends. Our main conclusions may be summarized as follows.

(i) There is a strong radial gradient in accretion time, which confirms that haloes are built from the inside out. Later accreting material settles farther from the centre of the halo; particles that

[3] The following numbers are insensitive to this choice.

[4] We assume $h = 0.73$ in order to compare with observations of the Milky Way.

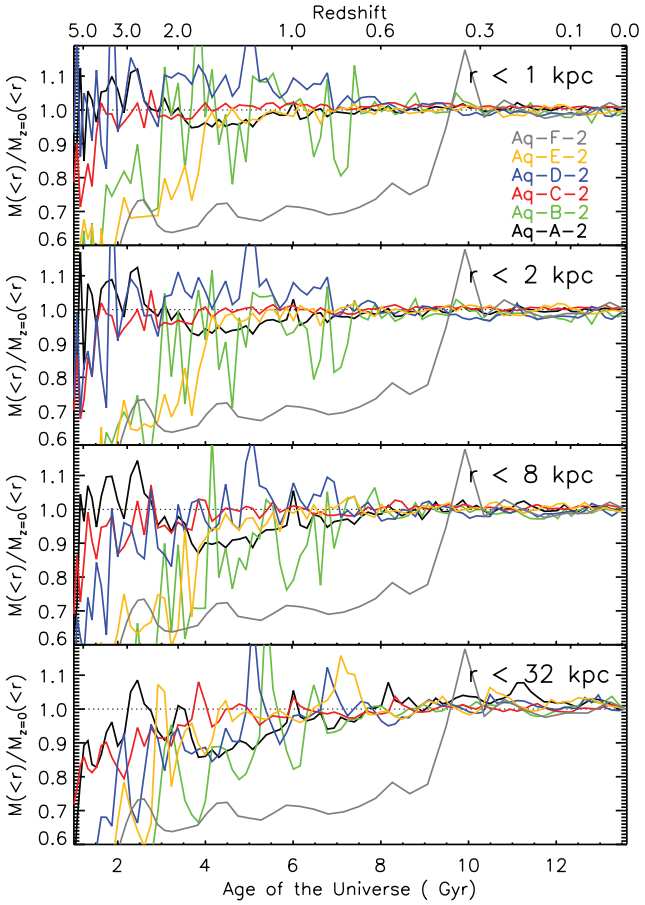

Figure 10. Total mass enclosed within different physical radii, $M\ (< r)$, for $r = 1$, 2, 8 and 32 kpc, as a function of cosmic time. Different colours correspond to different haloes, as labelled in the figure. Masses in each panel are normalized to their values at $z = 0$. Time is labelled at the bottom and redshift at the top. Except for halo Aq-F, which is the remnant of a recent major merger, the inner mass profile of Aquarius haloes has been very stable for the past 5–6 Gyr, a period comparable to the age of the Solar system.

today reside inside $10\,h^{-1}$ kpc are typically accreted ∼3 Gyr earlier than particles that reside at $100\,h^{-1}$ kpc from the centre.

(ii) Similarly, strong correlations exist between the distance of a particle from the halo centre and the mass at accretion of the progenitor halo which contained it. The innermost regions are dominated by particles brought in by massive clumps, 'major mergers' with mass ratios exceeding 1:10, as well as by those that joined the main progenitor at very early times ($z > 6$). Mass accreted diffusely and in minor mergers predominantly populates the more distant parts of the halo and dominates the total mass.

(iii) Minor mergers and diffuse accretion contribute approximately equally to the mass of each halo at each radius, at least at the resolution of our six Aquarius haloes where minor mergers can be distinguished up to mass ratios exceeding 10^6:1.

(iv) The inner mass profile of a halo is very stable at late times in systems that stay clear of major mergers. In five of the six Aquarius haloes, the profile within 32 kpc barely changed in the past 5–6 Gyr.

(v) Diffuse accretion contributes a substantial fraction of the final mass of the halo, roughly 30–40 per cent in our simulations. This is a robust result compatible with expectations from excursion-set modelling.

(vi) Our analysis shows that some of the material accreted smoothly had previously been part of other collapsed structures, from which it was probably ejected by mergers. The same mechanism leads a fair fraction of particles in the main halo to cycle in and out of its main progenitor; at $z = 0$ the cumulative mass of all particles 'associated' in the past with the main progenitor exceeds the final mass of the halo by at least 20 per cent.

(vii) Since photoionized gas is unable to collect in dark haloes with masses lower than about $10^8\,h^{-1}\,\mathrm{M}_\odot$ (which are well resolved in our simulations), baryons associated with such structures should remain diffuse after reionization until they are accreted into galaxies. Our estimates for dark matter diffuse accretion thus provide a lower limit to the fraction of baryons accreted smoothly into visible galaxies. As a result, more than half of all the baryons associated with the haloes of the Milky Way scale are expected to be accreted smoothly, rather than in clumps.

The inclusion of baryons and galaxy formation may alter our results quantitatively, but we expect the qualitative trends we have highlighted here to remain intact. Galaxy assembly is likely to lead to a steepening of the central gravitational potential and to a contraction of the dark halo, but it is unlikely to subvert the imprints of hierarchical growth on the radial structure of a halo. Confirming this expectation will have to await realistic hyrodynamical simulations of galaxy formation with resolution comparable to that of the present work.

These results emphasize the dynamic nature of halo build-up and provide insight into the radial structure of a halo and the history of its assembly process. The view that emerges highlights some misconceptions regarding hierarchical growth. CDM haloes are not passive repositories where mass is added in continuous but discrete events, but rather lively systems that can lose as well as gain material throughout their lifetimes. Diffuse accretion, recurring infall, escape and fallback are all processes that play important roles in the build-up of CDM haloes.

ACKNOWLEDGMENTS

The simulations of the Aquarius Project were carried out at the Leibniz Computing Center, Garching, Germany; at the Computing Centre of the Max-Planck-Society in Garching; at the Institute for Computational Cosmology in Durham; and on the 'STELLA' supercomputer of the LOFAR experiment at the University of Groningen. We thank Shaun Cole for providing us the code to produce Monte Carlo merger trees and Mike Boylan-Kolchin for useful comments and careful reading of the manuscript. JW acknowledges a Royal Society Newton International Fellowship, CSF acknowledges a Royal Society Wolfson Research Merit Award and AH acknowledges support from a VIDI grant by Netherlands Organisation for Scientific Research (NWO). AH acknowledges funding from the European Research Council under ERC-StG GALACTICA-240271. This work was supported by an STFC rolling grant to the Institute for Computational Cosmology.

REFERENCES

Angulo R. E., White S. D. M., 2010, MNRAS, 401, 1796
Balogh M. L., Navarro J. F., Morris S. L., 2000, ApJ, 540, 113
Benson A. J., Lacey C. G., Frenk C. S., Baugh C. M., Cole S., 2004, MNRAS, 351, 1215
Bett P., Eke V., Frenk C. S., Jenkins A., Helly J., Navarro J., 2007, MNRAS, 376, 215
Bond J. R., Cole S., Efstathiou G., Kaiser N., 1991, ApJ, 379, 440

Boylan-Kolchin M., Springel V., White S. D. M., Jenkins A., Lemson G., 2009, MNRAS, 398, 1150
Boylan-Kolchin M., Springel V., White S. D. M., Jenkins A., 2010, MNRAS, 406, 896
Cole S., Lacey C., 1996, MNRAS, 281, 716
Cole S., Helly J., Frenk C. S., Parkinson H., 2008, MNRAS, 383, 546
Davis M., Efstathiou G., Frenk C. S., White S. D. M., 1985, ApJ, 292, 371
Dekel A. et al., 2009, Nat, 457, 451
Diemand J., Kuhlen M., Madau P., 2007, ApJ, 667, 859
Efstathiou G., Frenk C. S., White S. D. M., Davis M., 1988, MNRAS, 235, 715
Fakhouri O., Ma C., 2010, MNRAS, 401, 2245
Genel S., Bouché N., Naab T., Sternberg A., Genzel R., 2010, ApJ, 719, 229
Gill S. P. D., Knebe A., Gibson B. K., 2005, MNRAS, 356, 1327
Helmi A., White S. D., Springel V., 2002, Phys. Rev. D, 66, 063502
Helmi A., White S. D. M., Springel V., 2003, MNRAS, 339, 834
Jenkins A., Frenk C. S., White S. D. M., Colberg J. M., Cole S., Evrard A. E., Couchman H. M. P., Yoshida N., 2001, MNRAS, 321, 372
Kauffmann G., White S. D. M., 1993, MNRAS, 261, 921
Kereš D., Katz N., Weinberg D. H., Davé R., 2005, MNRAS, 363, 2
Lacey C., Cole S., 1993, MNRAS, 262, 627
Ludlow A. D., Navarro J. F., Springel V., Jenkins A., Frenk C. S., Helmi A., 2009, ApJ, 692, 931
Madau P., Diemand J., Kuhlen M., 2008, ApJ, 679, 1260
Mo H. J., White S. D. M., 1996, MNRAS, 282, 347
Navarro J. F., Frenk C. S., White S. D. M., 1996, ApJ, 462, 563
Navarro J. F. et al., 2010, MNRAS, 402, 21
Okamoto T., Gao L., Theuns T., 2008, MNRAS, 390, 920
Parkinson H., Cole S., Helly J., 2008, MNRAS, 383, 557
Power C., Navarro J. F., Jenkins A., Frenk C. S., White S. D. M., Springel V., Stadel J., Quinn T., 2003, MNRAS, 338, 14
Press W. H., Schechter P., 1974, ApJ, 187, 425
Salvador-Sole E., Solanes J. M., Manrique A., 1998, ApJ, 499, 542
Spergel D. N. et al., 2003, ApJS, 148, 175
Springel V. et al., 2005, Nat, 435, 629
Springel V. et al., 2008a, MNRAS, 391, 1685
Springel V. et al., 2008b, Nat, 456, 73
Tasitsiomi A., Kravtsov A. V., Gottlöber S., Klypin A. A., 2004, ApJ, 607, 125
van Albada T. S., 1982, MNRAS, 201, 939
Wechsler R. H., Bullock J. S., Primack J. R., Kravtsov A. V., Dekel A., 2002, ApJ, 568, 52
White S. D. M., 1978, MNRAS, 184, 185
Zhao D. H., Jing Y. P., Mo H. J., Börner G., 2003, ApJ, 597, L9

This paper has been typeset from a TEX/LATEX file prepared by the author.